Chapter 12
Integrated Multigeneration Energy Systems

12.1 Introduction

Multigeneration, also called *polygeneration*, refers to energy systems that produce several useful outputs from one single or several kinds of primary energy input (viz. fuel). The purpose of multigeneration is to enhance the utilization of primary resources (fuels) and reduce the wasted energy. This is a method of improving the efficiency of energy generation processes for better sustainability. Less fuel is required to produce a given amount of electrical and thermal energy in a single unit than is needed to generate the same quantities of both types of energy with separate, conventional technologies (e.g., turbine-generator sets and steam boilers). Apart from generating "energy products" through a multigeneration system, one can also fabricate by-products with added value, such as carbon fibers and various chemicals.

Assume that one possesses a high-temperature thermal energy source (e.g., as obtained by fuel combustion or concentrated solar radiation). In a typical power generation application, the high-temperature heat is converted into work with heat engines. It is known from thermodynamics that only a part (limited by the Carnot factor) of the source heat can be converted into mechanical work, while the rest is wasted as low-temperature heat ejected into the environment. Therefore, the use of a primary energy source for generating one single product—power (or mechanical work)—is limited in terms of efficiency. The situation changes if the heat ejected by the heat engine is recovered and used for some purpose (e.g., space heating or water heating or industrial process heating). In such a case, the system cogenerates power and heat—two useful outputs from the primary energy (fuel) input. This is the simplest multigeneration system, known as cogeneration or a combined heat and power (CHP) system.

There are many possibilities for multigenerating valuable energy products from a single primary energy sources. Some examples are combined power and cooling; tri-generation of power cooling and heating; and multigeneration of hydrogen, oxygen, power, heating, cooling, and desalination. The multigeneration systems integrate several kinds of devices such as various kinds of heat engines, heat pumps, refriger-ation units, and hydrogen production units, and desalination units. For example,

gas turbines (GTs) can be integrated with solid oxide fuel cells to generate power and heating and enhance fuel utilization.

It is important to define the efficiency of multigeneration systems on a rational basis. But the difficulty comes from the fact that the outputs of the system are of several kinds. In order to determine the overall system output, it is not logical to simply add energies of different nature. For example, one cannot add electrical energy to thermal energy because their values are different: work is more valuable than heat. If heat and work are to be added, Carnot factors can be used for weighting the heat fluxes. Without recognizing the differences in these coproducts, as done by using associated exergy, possible improvements in the efficiency of cogeneration plants, or in their configuration within larger energy systems, can be missed; environmental benefits can also be wrongly interpreted. Furthermore, the attribution of costs and environmental emissions to the products of multigeneration systems is generally inappropriate when based on energy, as is commonly done, but it is appropriate, meaningful, and rational when it is based on exergy.

In this chapter, the theory of integrated multigeneration energy systems is reviewed with an emphasis on formulating the efficiency and the sustainability. The increase in efficiency and the corresponding decrease in fuel use by a multigeneration system, compared to other conventional processes for thermal, chemical, and electrical energy production, normally yield large reductions in greenhouse gas emissions. These reductions can be as large as 50% in some situations, while the same thermal and electrical services are provided. Several case studies are included.

12.2   System Integration

System integration in engineering entails combining several modules of subsystems into a larger system in which the subsystems work together to achieve better effectiveness or efficiency. There are many examples of system integration in energy technology:

- Cascading gas turbine cycles with bottoming Rankine cycles for improved efficiency of power generation
- Integrating a solid oxide fuel cell with gas turbine cycles for better fuel utilization and enhanced power production efficiency
- Using coal gasification coupled to gas turbine generators, again for better power generation efficiency
- Work recovery from the exhaust gas of vehicle engines to drive turbochargers and enhance the combustion process and fuel utilization for better propulsion efficiency

To elucidate the concept of integration, we present here a typical case from sustainable energy engineering, namely, the integration of a gas turbine cycle with solid oxide fuel cells (SOFCs). This topic has been extensively investigated as a mean of enhancing the thermodynamic efficiency of power production.
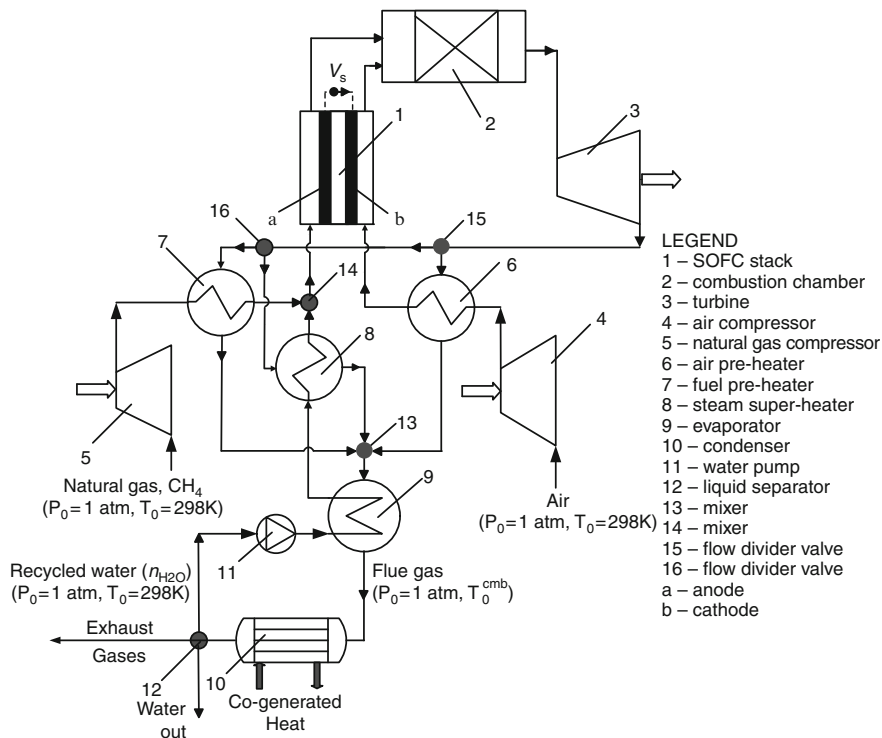
Fig. 12.1 Integrated SOFC–gas turbine cogeneration system with methane conversion [modified from Dincer et al. (2010)]

An interesting characteristic of SOFC is the application of yttrium-stabilized zirconia anodes that permit conversion on their surface of methane into synthesis gas (hydrogen and carbon monoxide). The synthesis gas is more efficient than natural gas (methane) as a fuel in gas turbines, and furthermore cascading SOFC with gas turbines allows for a very efficient fuel utilization. We present an integration scheme of gas turbines and SOFC for cogeneration of power and heat. The treated system is adapted from the one proposed by Granovskii et al. (2007, 2008) and Dincer et al. (2010) by modifying it to a cogeneration system. As mentioned in Dincer et al. (2010) SOFC–gas turbine cycles with cogeneration have the potential of achieving 66% utilization efficiency.

Figure 12.1 introduces the proposed system. As can be seen, the system generates three outputs: DC electric current by the fuel cell stack (label 1), shaft rotation power by the gas turbine (label 3), and low-temperature heat—used for heating purposes—by the steam condenser (label 10). Note that the figure shows the work inputs (in the compressors) and outputs (from the turbine) with block arrows. Looking at the integrated system diagram, one can observe that this is a kind of Brayton cycle, including two compressors (for air and natural gas) and a turbine; in between is interlaced the SOFC, which plays the role of an "active" preheater that
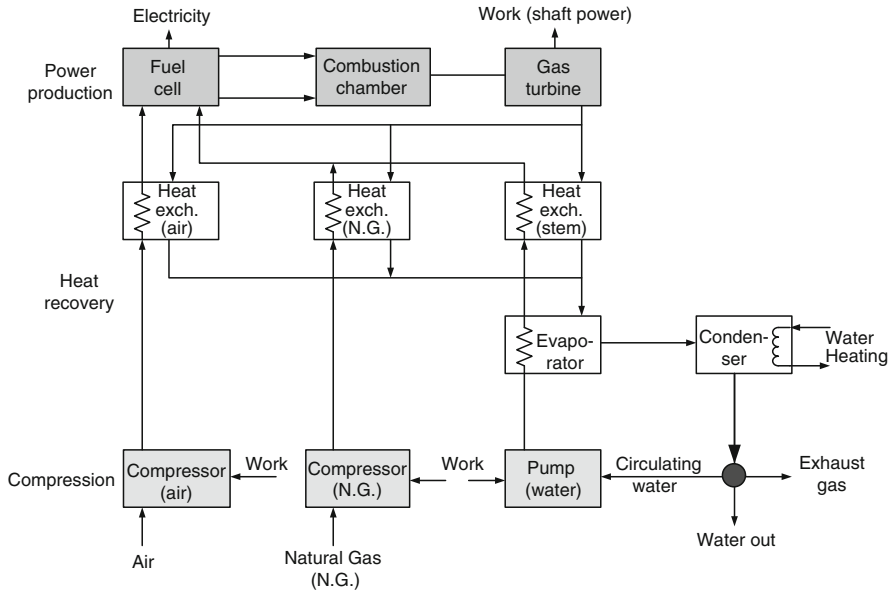
Fig. 12.2 Operational modules of the integrated SOFC–gas turbine system [modified from Dincer et al. (2010)]

generates electricity while consuming some of the energy of the primary fuel and is followed by a combustor, where the fuel energy is utilized fully. Water is recovered from exhaust gases by cooling and condensing. Part of the resulting heat is used internally in the steam evaporator (label 9) and steam super-heater (label 8) while the condenser rejects the heat in the exterior; this heat is recovered by a stream of water and represents the cogenerated (useful) heat.

The system can be divided in three operational modules as indicated in Fig. 12.2, namely: (1) the compression section (bottom); (2) the heat recovery section (middle); and (3) the power production section (top), which comprises the fuel cell stack and the gas turbine. Several assumptions for thermodynamic modeling of the system were considered, such as that the values of pressure and temperature (T_0, P_0) of the reference environment are taken as standard, the inlet temperature in the SOFC is taken as 1,073 K and the outlet as 1,273 K (based on the literature, these values are advantageous with regard to SOFC efficiency), and the gas turbine output temperature is taken as 1,123 K to provide at least a 50°C temperature difference at the heat exchanger inlets.

The isentropic efficiency of the turbine is assumed to be 93% and that of the compressors 85%, while the air composition is considered to be 21% oxygen and 79% nitrogen. Energy losses due to fluid friction are ignored; the water pump work is also ignored because it is significantly small with respect to produced power; the chemical reactions are assumed to be at equilibrium.

The modeling starts by analyzing the chemical reactions at the level of SOFC (which is regarded as a "black box"); these reactions are

$$
\begin{cases}
CH_4 + 2O_2 \rightarrow CO_2 + 2H_2O(g) - 802 \,\text{kJ/mol} \\
CH_4 + H_2O \leftrightarrow CO + 3H_2 + 206 \,\text{kJ/mol} \\
CO + H_2O \leftrightarrow CO_2 + H_2 + 41 \,\text{kJ/mol}
\end{cases}
. \qquad (12.1)
$$
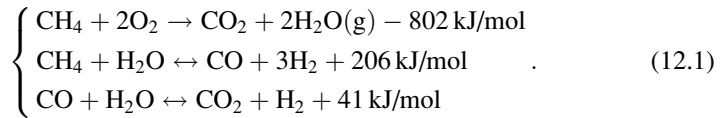
The chemical equilibrium equations for methane reforming at the fuel cell anode give the equilibrium constants that correspond to the methane steam reaction and the carbon monoxide steam reaction listed above. According to these chemical equations, the reaction constants become

$$
\begin{cases}
K_{CH_4} = \dfrac{\left[P_{H_2}^3 P_{CO}\right]}{\left[P_{CH_4} P_{H_2O}\right]}, \\[3mm]
K_{CO} = \dfrac{\left[P_{H_2} P_{CO_2}\right]}{\left[P_{CO} P_{H_2O}\right]},
\end{cases}
\qquad (12.2)
$$

where P is the partial pressure of the component.

Mass, molar, energy, entropy, and exergy balances are written for each component of the system. The SOFC stack exergy efficiency η_s is expressed as a percentage of the Gibbs free energy change, $W_e = -\eta_s \Delta G_1$, where ΔG_1 is the Gibbs free energy difference between the output and input flows, that is, $\Delta G_1 = G_1^{out} - G_1^{in}$. The Gibbs free energy of a component in a gaseous mixture can be written as $G_i = H - TS_i$ and $S_i = S_i^0 - R \ln(P_i)$, where H_i and S_i represent the molar enthalpy and entropy of a component at $P_0 = 1$ atm, and P_i denotes partial pressure, T the temperature, and R the universal gas constant. The thermal efficiency η_s is related to the open-circuit fuel cell voltage $V_s = W_e/(n_{O_2} n_e F)$, where n_{O_2} is the number of moles of oxygen that traverse the fuel cell electrolyte, n_e is the number of moles of electrons transmitted to a circuit chain per mole of oxygen, and F is the Faraday constant.

The output flows of the SOFC stack are the input flows to the combustion chamber. Anode exhaust and oxygen-depleted air from the SOFC enters the combustion chamber, and combustion products exit. Sufficient oxygen is provided for complete combustion of the CH_4, H_2, and CO from the SOFC stack. The temperature of the input flows is the same as that of the air and methane exiting the SOFC stack. An energy balance can be determined for the adiabatic combustion chamber ($\Delta H_2 = 0$). The exergy destroyed by each component is calculated with $Ex_{d,i} = T_0 \Delta S_i$, where i is the index of the component as indicated in Fig. 12.1.

By applying the general efficiency equations for utilization efficiency and for exergy efficiency, the cogeneration efficiencies of the overall system may be calculated; the particular forms of the efficiency equations are in this case
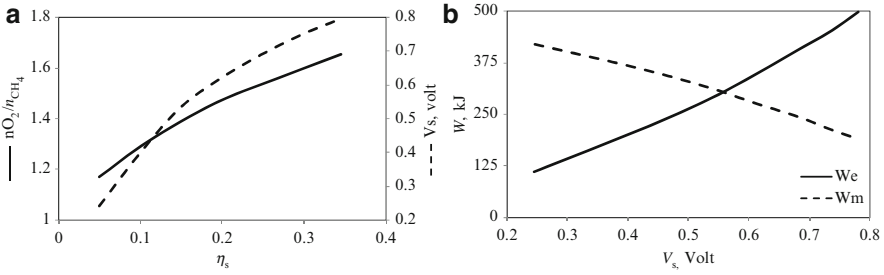
Fig. 12.3 The effect of the air/fuel ratio on fuel cell stack efficiency (**a**), and voltage and power output (**b**); W_e fuel cell power output; W_m net turbine power output, both per mol of fuel [data from Dincer et al. (2010)]

$$\begin{cases} \eta = \dfrac{\dot{W}_{FC} + \dot{W}_T + \dot{Q}_C}{\dot{m}_{CH_4} LHV_{CH_4}}, \\[3mm] \psi = \dfrac{\dot{W}_{FC} + \dot{W}_T + \dot{Q}_C(1 - T_0/T_C)}{\dot{m}_{CH_4} \dot{Ex}^{ch}_{CH_4}}, \end{cases} \qquad (12.3)$$

where $\dot{Q}_C$ is the heat recovered from the condenser. As mentioned above, the energy efficiency can be referred to the lower or higher heating value of the fuel depending on the case. In this analyzed case, the water is expelled out of the system both in liquid form and as steam; however, the portion that comes from methane–fuel utilization is expelled as steam; thus, the reference for utilization efficiency is the lower heating value (LHV) of methane.

For better overall efficiency, it is important to adjust the molar flux of air and fuel such that the operational-circuit fuel cell voltage is the highest. Figure 12.3 shows the results regarding the variation of the voltage and the power output of the fuel cell stack and the net turbine work correlated with the air (oxygen)/fuel ratio. To avoid carbon deposition on the anode surface, the molar ratio of methane to steam should exceed 1:2. Values of V_s greater than 0.7 V are therefore unsuitable for the system considered here.

Note that the maximum efficiency of an SOFC stack does not coincide with the maximum thermodynamic efficiency. The cost of SOFC stacks is a limiting factor, and their operation at higher work densities reduces the power generation cost for the overall system. This observation, along with the fact that the work output from the methane conversion catalyst is stable when the steam–methane ratio ranges between 2:1 and 3:1, suggests that the most beneficial SOFC operating conditions occur for V_s of 0.4 to 0.7 V. Then, the energy efficiency of the overall system is seen to be 70% to 80%, respectively.

For the numerical example assumed in Dincer et al. (2010), the operational cell voltage is taken to be 0.61 V and the fuel cell stack energy efficiency is 20%. In these conditions, the calculated exergy destructions for each component are depicted in Fig. 12.4. The exergy destruction in the condenser is small because of the reduced level of temperature (close to T_0) and is negligible with respect to that
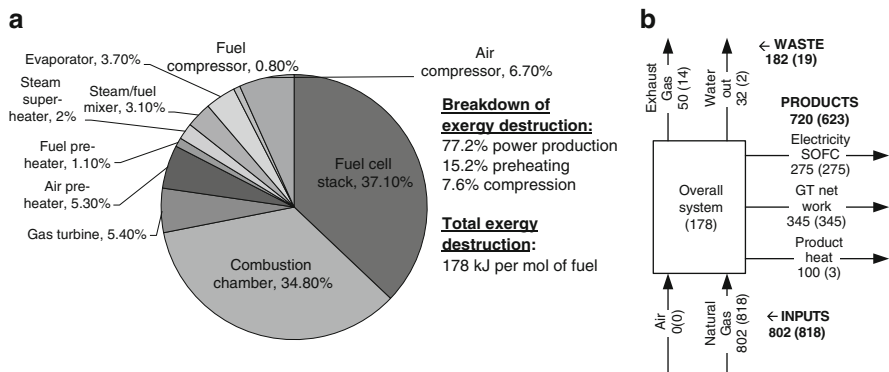
Fig. 12.4 The destruction of exergy in various components (**a**) and the overall outputs (**b**) of the SOFC/GT system [data from Dincer et al. (2010)]

of other components. Also, because the pump work is ignored, (as justified above), the exergy destruction in the pump is nil.

The efficiency of power production only of the integrated system can be estimated from the efficiency of the SOFC itself, which becomes $\eta = 275/802 = 34.2\%$ and $\psi = 275/818 = 33.6\%$.

12.3 Multigeneration

The above example of an integrated SOFC and gas turbine demonstrated that the power production efficiency increases because of the integration of two technologies. There we calculated the efficiencies of power production only. However, as mentioned, the system cogenerates useful heat. The overall efficiency of the system with cogeneration, calculated according to Eq. (12.3) is $\eta = 720/802 = 90\%$ (for fuel utilization) and $\psi = 623/818 = 76\%$ (for exergy conversion). Thus, the gain in efficiency due to cogeneration is about 56% in fuel utilization terms and about 43% in terms of exergy. This example demonstrates the important benefit of multiple energy system integration (viz. fuel cells and gas turbines) and multigeneration. Multigeneration can potentially generate even better efficiencies than cogeneration.

Figure 12.5 presents the general layout of an integrated multigeneration system, which shows that from a primary energy input several useful outputs are obtained. Basically, these systems could integrate various conversion technologies to produce commodities from a primary source of a single kind.

According to the definition, the efficiency of a multigeneration system can be expressed as the ratio of useful output(s) to the consumed primary energy at input. As mentioned above, the outputs can be of different kinds (electric power, heat, synthetic fuel, and others). Therefore, the energy outputs must be converted
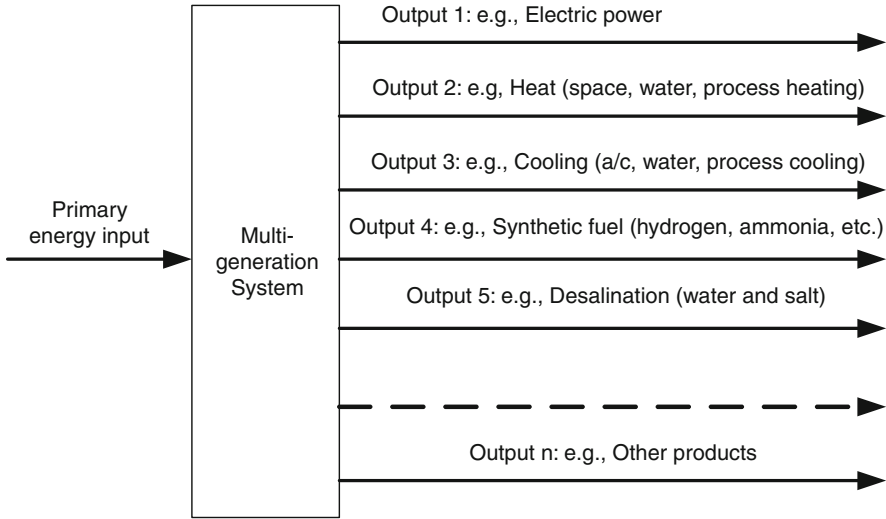
Fig. 12.5 General layout of an integrated multigeneration system

first into similar forms of energy (e.g., work, heating value) and then summated. One can, for example, express the outputs and the inputs in terms of energy content. Thus, the energy-based efficiency is obtained. A fairer approach is to express each output and the input in terms of exergy. Adding exergies is more meaningful than energy contents because one operates with quantities of the same kinds, namely, mechanical work equivalents. Another possibility of quantifying the performance of multigeneration systems is to express each stream (outputs, inputs) through costing equivalents. One obtains thus an economic effectiveness showing the ratio between the product's price (output 1 to output n in Fig. 12.5) versus the fuel consumption cost. Furthermore, the ecological impact of the system can be calculated by considering the equivalent pollutant emissions (viz. greenhouse gases, etc.) per unit of primary energy consumption or per unit of total product.

With reference to Fig. 12.5, the typical expression for the system energy efficiency can be exemplified as follows:

$$\eta = \frac{W + Q_{\mathrm{H}} + Q_{\mathrm{C}} + \mathrm{HHV}_{\mathrm{SF}} + H_{\mathrm{salt}} + H_{\mathrm{OP}}}{\mathrm{HHV}_{\mathrm{PF}}}, \qquad (12.4)$$

where the outputs are expressed in terms of energy, W is the work (or electric power), Q_{H} and Q_{C} are the energy in the form of heat used for heating and cooling, respectively, $\mathrm{HHV}_{\mathrm{SF}}$ is the caloric energy embedded in the synthetic fuel (based on its higher heating value), H_{salt} is the equivalent energy embedded in the produced salt, and H_{OP} is the energy in other products; the input is expressed with respect to the higher heating value of the consumed primary fuel (or primary energy source) as $\mathrm{HHV}_{\mathrm{PF}}$. Observe that the water produced by desalination is not included in Eq. (12.4) at the numerator; this is due to the fact that the equivalent energy

embedded in water is nil (water can neither be combusted nor reacted with the standard environment to generate energy).

Efficiency equations similar to Eq. (12.4) can be developed for each particular case. For example, in the case of cogeneration of electric power and heat, the energy efficiency expression is

$$\eta = \frac{W + Q_H}{[m_{PF}HHV_{PF}]}. \tag{12.5}$$

Note that Kanoglu and Dincer (2009) refer to Eqs. (12.4) and (12.5) as the "utilization efficiency" to differentiate it from the thermal efficiency, which is commonly used for a power plant with a single output, power. As also pointed out above, it is inappropriate to summate commodities that are different [like the addition of power and heating in Eq. (12.5)], although work and heat both have units of energy. The exergy efficiency of the general system from Fig. 12.5 is given according to general exergy analysis methodology (Dincer and Rosen 2007) by

$$\psi = \frac{W + Ex_H + Ex_C + m_{SF}ex_{SF}^{ch} + m_{salt}ex_{salt}^{ch} + Ex_{OP}}{m_{PF}ex_{PF}^{ch}}, \tag{12.6}$$

where $Ex_{H,C}$ are the exergy equivalent of heat and cooling produced ($Q_{H,C}$), m_{SF} is the quantity of produces synthetic fuel having the exergy ex_{SF}^{ch}, $m_{salt}ex_{salt}^{ch}$ is the exergy content associated with salt resulting from desalination, and Ex_{OP} is the exergy associated with other products; the consumed primary fuel is m_{PF} having the specific chemical exergy ex_{PF}^{ch}. The exergy associated with the generated heating and cooling $Ex_{H,C}$ is expressed with the help of Carnot factor; in general, assuming a variable heat transfer process, this exergy is

$$Ex_{H,C} = \int \delta Q \left(1 - \frac{T_0}{T}\right). \tag{12.7}$$

Here, T is the temperature at which heat is transferred. This relation is of little practical value unless the functional relationship between the rate of heat transfer ($Q_{H,C}$), heat flux, and temperature T is known. In many cases, heat is utilized by transferring it from the working fluid exiting the heat or cooling producing device (e.g., turbine, internal combustion engine, heat pump, refrigeration evaporator) to a secondary fluid, in a heat exchanger. Therefore, the exergy rate of heating or cooling $\dot{E}x_{H,C}$ can be expressed as exergy variation in working fluid (or heat transfer fluid, depending on the case):

$$\dot{E}x_{H,C} = \dot{m}_{WF}(\Delta h - T_0 \, \Delta s)|_{WF}, \tag{12.8}$$

where index WF stands for "working fluid" and h and s represent the specific enthalpy and entropy, while $\dot{m}$ is the mass flow rate.
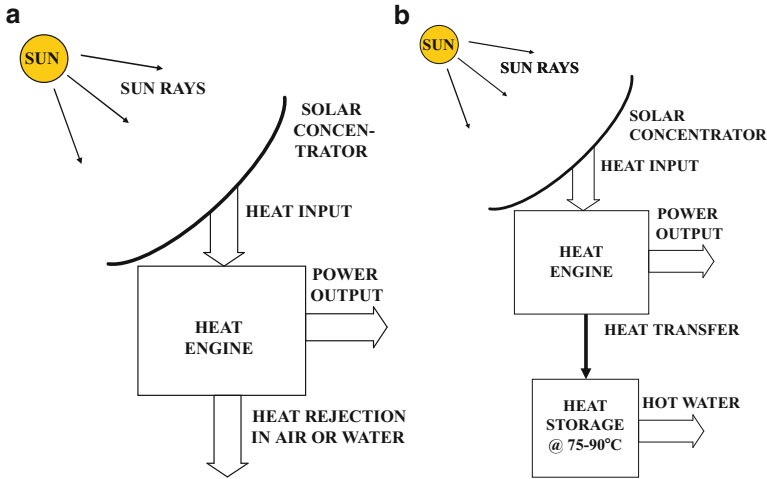
Fig. 12.6 Concentrated solar energy systems: (**a**) solar power and (**b**) solar power and hot water

In order to better illustrate the application of Eqs. (12.4) and (12.6) for energy and exergy efficiency of multigeneration system, we analyze now a number of relevant examples. We start with the system presented in Fig. 12.6a, which represents a concentrated solar power system, where concentrated solar radiation is used to drive a heat engine.

The energy efficiency of system (a) is given by $\eta = W/I_{sun}$, where W is the electric power output and I_{sun} is the total direct bean radiation input. The exergy associated with I_{T_0} is the exergy of solar radiation and is $I_{sun}(1 - T_0/T_{sun})$, where T_{sun} is the temperature of the solar radiation. Therefore, the exergy efficiency of system (a) is $\psi = W/[I_{sun}(1 - T_0/T_{sun})]$. The typical values for the practical system are 20% for η and 21% for ψ. Now, if the rejected heat by the heat engine is recovered and used to heat water, as illustrated in Fig. 12.6b, the corresponding energy and exergy efficiency are, respectively, $\eta = (W + Q_H)/I_{sun}$ and $\psi = (W + Ex_H)/[I_{sun}(1 - T_0/T_{sun})]$, where Ex_H can be estimated with Eq. (12.7) or (12.8); in the case that the temperature variation at the heat engine sink is nil or negligible, the exergy associated with heat exchange is given by

$$Ex_H = Q_H\left(1 - \frac{T_0}{T_H}\right). \tag{12.9}$$

Example

In order to illustrate the application of Eq. (12.8), let us consider a particular heat engine for the cogeneration system illustrated in Fig. 12.6b. A simple cogeneration heat engine can be a steam power plant with steam extraction. This is presented in Fig. 12.7; this heat engine can be supplied with "primary fuels" other than solar radiation (e.g., coal). Therefore, the energy associated with the primary energy source is either I_{sun} for the solar concentrator system or, more generally, is
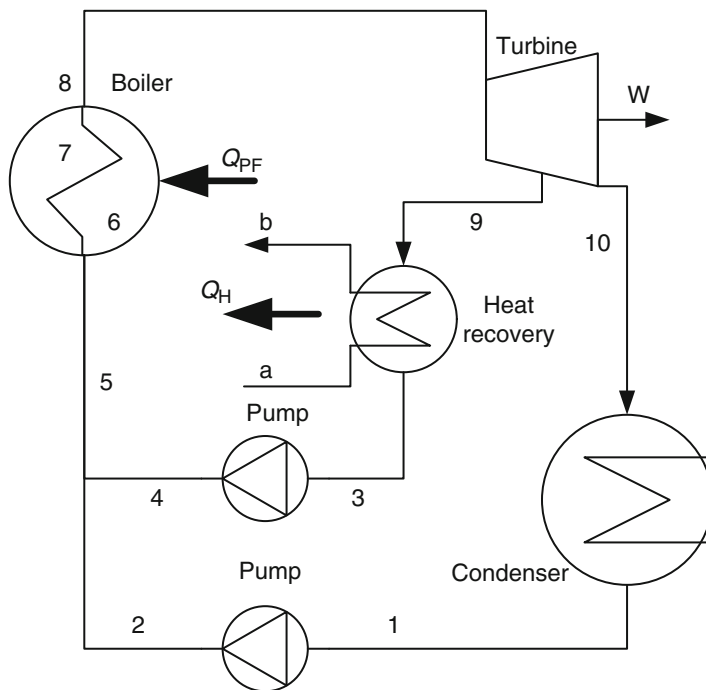
Fig. 12.7 Steam heat engine with cogeneration

$m_{PF}HHV_{PF}$, where m_{PF} is the quantity of fuel consumed per unit of energy output; this energy and the useful product energies can be expressed also as a rate, for example, $\dot{m}_{PF}HHV_{PF}, \dot{Ex}_{H}$. For the numerical example considered here, we assume that the power plant operates with steam that boils at 300°C and is superheated up to 450°C in a solar collector. The condensation is at 40°C, and the condenser for heat recovery operates at 80°C.

At states 1 and 3 of the cogeneration heat engine, one assumes saturated liquid. Moreover, one assumes that 50% of the expanded flow is extracted from the turbine in state 9 and used for heat cogeneration. Engineering Equation Solver (EES) is used to estimate the thermodynamic properties of the steam (though simple steam tables could be used for cycle calculation). The calculation of the thermodynamic cycle is done with the purpose of determining pressure, temperature, entropy, enthalpy, and specific exergy, all in state point, and eventually calculating the overall efficiency. The calculation proceeds by writing energy and mass balance equations for each component and relevant equations for each state as follows:

- Flow fraction is $f = 0.5$; the flow division fraction is defined based on mass balance equations, namely, $\dot{m}_8 = \dot{m}_9 + \dot{m}_{10}$; $\dot{m}_5 = \dot{m}_4 + \dot{m}_2$; $\dot{m}_{10} = \dot{m}_1 = \dot{m}_2$; $\dot{m}_9 = \dot{m}_3 = \dot{m}_4$. The flow division is defined as $f = \dot{m}_4/\dot{m}_5 = \dot{m}_9/\dot{m}_8$.
- State 1: $T_1 = 40$°C, $x_1 = 0$, and $f = 0.5$, one evaluates the specific enthalpy to $h_1 = 167.5$ kJ/kg, total flow enthalpy $h_{t1} = 83.75$ kJ/kg of stream 5–8, pressure $P_1 = 74$ mbar, and specific entropy $s_1 = 572$ J/kg K.

- State 2: Pressure is the same as in state 6 (saturated liquid at 300°C), $P_2 = P_6$ = 86 bar, isentropic efficiency of the pump is assumed $\eta_{P1} = 0.8$ and defined by the equation $\eta_{P1} \times (h_{2s} - h_1) = h_2 - h_1$, where $h_{2s} = h(P_2, s_1) = 176.1$ kJ/kg is the specific enthalpy for isentropic pressurization; thus, $h_2 = 174.4$ kJ/kg and $s_2 = 567$ J/kg K.
- State 3: It is assumed that condensation is at 80°C, thus $T_3 = 80$°C and $x_3 = 0$; the specific enthalpy is $h_3 = 334.9$ kJ/kg and the total enthalpy $h_{t3} = (1 - f)$ $h_3 = 167.5$ kJ; the pressure of saturated liquid is $P_3 = 0.474$ bar and specific entropy $s_3 = 1,075$ J/kg K.
- State 4: This is a pressurized liquid state at $P_4 = P_6 = 86$ bar. The pump efficiency is $\eta_{P2} = 0.8$ and the pump equation is $\eta_{P2} \times (h_{4s} - h_3) = h_4 - h_3$, which is solved for h_4 for known isentropic process enthalpy $h_{4s} = 343.7$ kJ/kg, thus $h_4 = 341.9$ kJ/kg and $h_{t4} = 171$ kJ.
- State 5: We have the energy balance $h_5 = h_{t5} = h_{t4} + h_{t2} = 258.2$ kJ/kg while $P_5 = P_6$, $T_5 = T(h_5, P_5) = 60$°C, and $s_5 = 826$ J/kg K.
- State 6: We have saturated liquid ($x_6 = 0$) at $T_6 = 300$°C and $h_6 = h_{t6}$ 1,344 kJ/kg.
- State 7: Saturated vapor is at $x_7 = 1$, $P_7 = P_6$, $h_7 = 2,749$ kJ/kg, and $s_7 = 5,704$ J/kg K.
- State 8: Superheated vapor is at $P_8 = P_6$, $T_8 = 450$°C, $h_8 = h_{t8} = 3,263$ kJ/kg, and specific entropy $s_8 = 6,513$ J/kg K.
- State 9: Expansion to intermediate pressure $P_9 = P_3$; turbine's isentropic efficiency is assumed $\eta_T = 0.8$, and turbine equation is $\eta_T \times (h_8 - h_{9s}) = h_8 - h_9$, where $h_{9s} = h(P_9, s_8) = 2,255$ kJ/kg and $h_9 = 2,457$ kJ/kg; the total enthalpy is $h_{t9} = 1,228$ kJ; the specific entropy is $s_9 = 7,084$ J/kg K.
- State 10: Expansion at lowest pressure $P_{10} = P_1$, assuming $\eta_T = 0.8$ and $\eta_T \times (h_8 - h_{10s}) = h_8 - h_{10}$; thus, $h_{10} = 2,275$ kJ/kg and $h_{t10} = 1,138$ kJ.
- All calculations are done for a main flow rate of 1 kg/s. The electric power generation efficiency is given by $\eta_E = \dot{W}_{net}/\dot{Q}_{PF}$, where $\dot{W}_{net} = \dot{W}_T - \dot{W}_{P1} - \dot{W}_{P2}$.
- Using the total enthalpies, one can determine the work generated and consumed by the turbine and pumps, respectively, and also the energy consumed by the primary fuel. One obtains $\eta_E = 30\%$.
- For the system with cogeneration, the fuel utilization efficiency is given by $\eta_{cog} = (\dot{W}_{net} + \dot{Q}_H)/\dot{Q}_{PF}$, for which one obtains 65%.
- The exergy efficiency is based on the exergy input in the system, which can be calculated with $\dot{Ex}_{PF} = h_8 - h_5 - T_0(s_8 - s_5) = 1,310$ kJ.
- Thus, the exergy efficiency of electric power generation is $\psi_E = \dot{W}_{net}/\dot{Q}_{PF} = 68\%$; also, the exergy efficiency of the cogeneration system is calculated accounting for the cogenerated heat exergy, $\dot{Ex}_H = (1 - f)$ $\times [h_9 - h_3 - T_0(s_9 - s_3)] = 165.6$ kJ. The cogeneration exergy efficiency becomes $\psi_{cog} = (\dot{W}_{net} + \dot{Ex}_H)/\dot{Ex}_{PF} = 80\%$.

The heat recovered from the heat engine is indicated in the figure with Q_H and can be expressed based on the enthalpy of the stream a–b, that is $\dot{Q}_H = \dot{m}_{ab}(h_b - h_a)$; then, the cogeneration energy efficiency is

$$\eta = \frac{\left[\dot{W} + \dot{m}_{ab}(h_b - h_a)\right]}{\dot{m}_{PF}HHV_{PF}} \qquad (12.10)$$

and the exergy efficiency becomes

$$\psi = \frac{\dot{W} + \dot{m}_{ab}[h_b - h_a - T_0(s_b - s_a)]}{\dot{m}_{PF}Ex_{PF}}, \qquad (12.11)$$

where the term $h_b - h_a + T_0(s_b - s_a)$ represents the specific exergy of the heat transfer fluid, ex_{HT}. This term can be rearranged as $ex_{HT} = (h_b - h_a)\{1 - T_0/[(h_b - h_a)/(s_b - s_a)]\}$.

If the temperature at which heat transfer occurs is constant, that is, $T_a = T_b = T_H$, then one can express the entropy variation simply as $s_b - s_a = (h_b - h_a)/T_H$. The case when the heat is transferred to a phase-change material is a good example of a situation when heat transfer occurs at a constant temperature. In such cases, the Carnot factor $(1 - T_0/T_H)$ can be within the expression of exergy efficiency. Therefore, the exergy efficiency becomes

$$\psi = \frac{\dot{W} + \dot{m}_{ab}(h_b - h_a)(1 - T_0/T_H)}{\dot{m}_{PF}Ex_{PF}}. \qquad (12.12)$$

Typically, for the system from Fig. 12.6b, the cogeneration efficiency values are 60% to 80% for energy and about 30% to 35% for exergy. If sources other than solar radiation are used, the energy-based efficiency (or utilization efficiency) can be even higher, up to 90% to 98%. The high utilization efficiency is obtained by insulating the system well, so that all produced thermal energy is recovered and used. In a solar concentrating system, perfect insulation is not possible, and various losses such as optical and thermal radiation impede obtaining utilization efficiencies higher than about 80% to 85%. For systems using fuel combustion, it is possible to devise better insulation so that less primary energy is lost. Typical efficiency figures for various heat engines with cogeneration are shown in Table 12.1. It is assumed that the cogenerated heat is used for water heating, where the stream of water at the inlet (state a in Fig. 12.7) is assumed to be 50°C and at the outlet (state b) 90°C.

Other typical systems for cogeneration of heat and power are suggested Fig. 12.8. For systems (a) and (b), Eqs. (12.10) and (12.11) can be applied to determine the utilization and exergy efficiencies, respectively. In the case of a

Table 12.1 Typical efficiencies of various cogeneration systems

Efficiency	Concentrated solar (%)	Steam engine (%)	Gas power plant (%)	Diesel engine (%)	Geothermal plant (%)
Utilization	70–80	48	47	78	16
Exergy	30–35	23	23	48	44
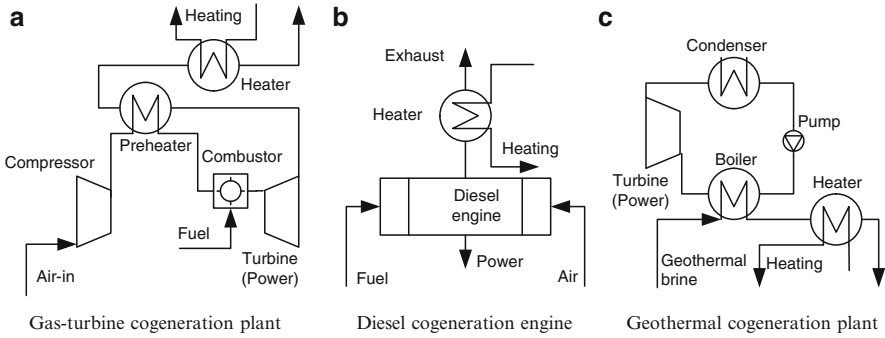
Fig. 12.8 Some typical cogeneration systems

geothermal system, the energy and exergy content of the primary source, which is geothermal brine, can be calculated by assuming that the brine is cooled down to the ambient temperature. Denoting (h_0, s_0) the specific enthalpy and entropy of the brine at environmental temperature T_0, the associated primary energy and exergy become

$$\begin{cases} \dot{Q}_{\text{geo}} = \dot{m}_{\text{geo}}(h_{\text{geo}} - h_0), \\ \dot{Ex}_{\text{geo}} = \dot{m}_{\text{geo}}[h_{\text{geo}} - h_0 - T_0(s_{\text{geo}} - s_0)], \end{cases} \tag{12.13}$$

where subscript "geo" stands for "geothermal" and h_{geo}, s_{geo} are the specific enthalpy and entropy, respectively, of the hot geothermal brine.

Some multigeneration systems are suggested here by expanding the concentrated solar cogeneration plant from Fig. 12.6b. Thus, Fig. 12.9a shows a system with tri-generation, where the outputs are power, hot water, and space heating. Heat storage can be applied in order to store solar energy in the form of thermal energy for overnight heating.

The system from Fig. 12.9b is an extension of the tri-generation system to multigeneration. In this case, the system produces power heating and cooling, where cooling is used for air conditioning and other purposes (like food preservation) and heating is used for space and water. Such a system thus generates five useful outputs. The exergy efficiency can be written as

$$\psi = \frac{\dot{W} + \dot{Q}_{\text{HW}}(1 - T_0/\bar{T}_{\text{HW}}) + \dot{Q}_{\text{SH}}(1 - T_0/\bar{T}_{\text{SH}}) + \dot{Q}_{\text{C}}(1 - T_0/\bar{T}_{\text{C}}) + \dot{Q}_{\text{AC}}(1 - T_0/\bar{T}_{\text{AC}})}{I_{\text{sun}}(1 - T_0/T_{\text{sun}})}, \tag{12.14}$$

where indices HW, SH, C, and AC mean hot water, space heating, cooling, and air conditioning, respectively. The average process temperature $\bar{T}$ has been used to express the Carnot factors used for expressing the exergy of heat fluxes. This approximation is valid if the temperature does not vary much. With the system in Fig. 12.9b, one can achieve 35% exergy efficiency while utilization efficiency can
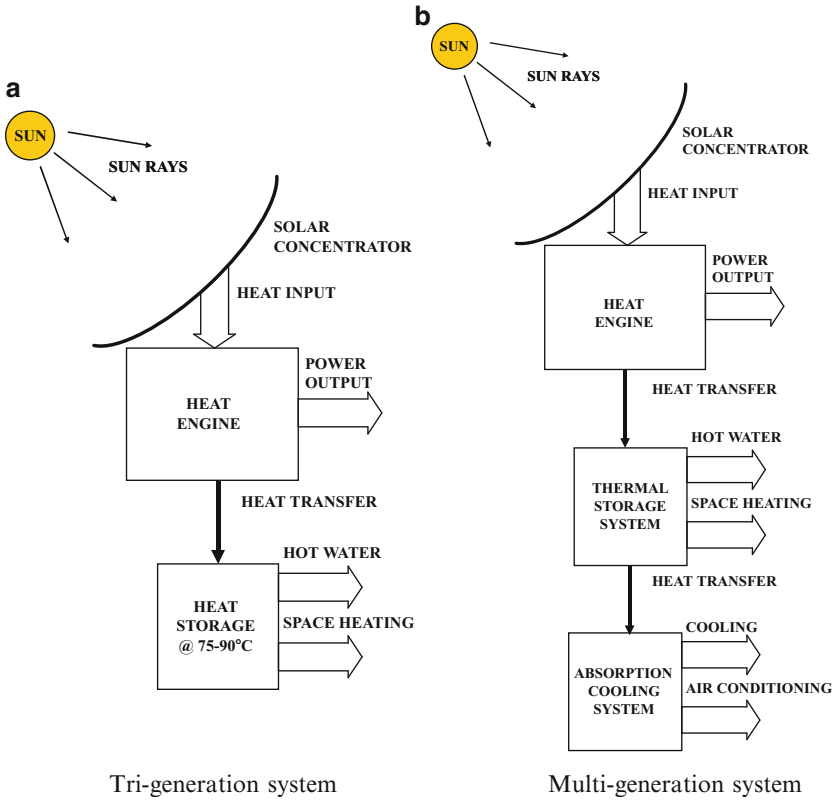
Fig. 12.9 Examples of tri- and multigeneration hybrid concentrated solar power systems

reach, in principle, 90%. The system integrates several components such as the heat engine, heat recovery heat exchangers, thermal storage system, and an absorption refrigeration system.

The system suggested in Fig. 12.10 integrates a solar-driven heat engine with an electrolyzer that produces hydrogen and oxygen from water and an absorption refrigeration system that generates cooling from heat recovery from the heat engine; in addition, there is a thermal storage system and a heat recovery system that delivers heating as useful product for heating water and some other needs. The energy efficiency of the system from Fig. 12.10a is

$$\eta = \frac{\left(\dot{W} + \dot{m}_{H_2}\text{HHV}_{H_2} + \dot{Q}_{HW} + \dot{Q}_{SH} + \dot{Q}_C + \dot{Q}_{AC}\right)}{I_{sun}}. \qquad (12.15)$$

In Eq. (12.15), the term $\dot{m}_{H_2}$ denotes the production rate of hydrogen. A part of the produced electricity is used to drive the electrolyzer, which produces hydrogen and oxygen from water during the day. In the nighttime, the stored hydrogen can be used in a fuel cell to generate electricity. Thus, one can have a continuous production of electricity for 24 hours.
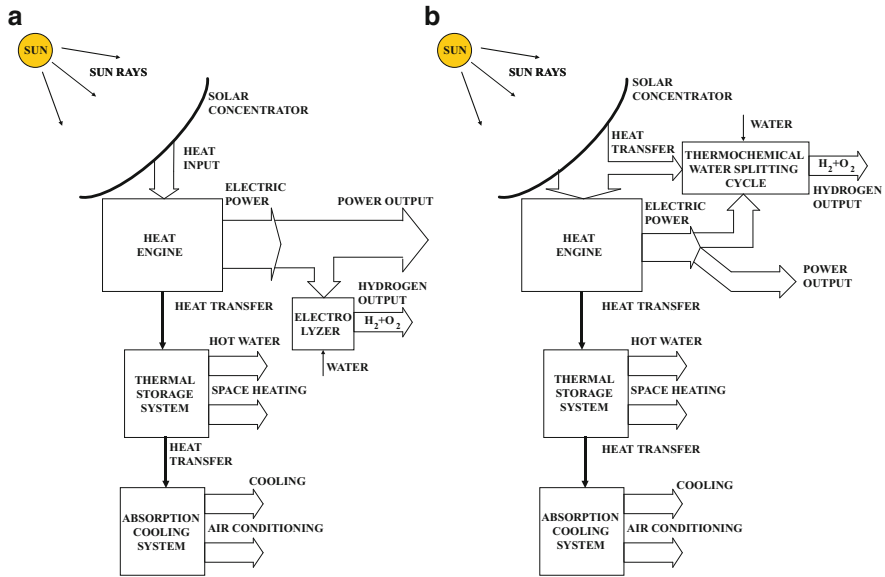
Fig. 12.10 Solar-driven multigeneration hybrid systems with hydrogen production (**a**) by electrolysis and (**b**) by thermochemical water splitting

An alternative to the system from Fig. 12.10a is presented in Fig. 12.10b, where the electrolyzer is replaced by a thermochemical water splitting plant. The thermochemical water splitting process consumes less primary thermal energy than the electrolyzer because it does not require any electricity or it requires much less electricity. Therefore, the generation of electricity to drive the water splitting process (or at least substantially reduce the required electricity for it) is avoided with the benefit of improving energy utilization and exergy efficiency. Rough calculations indicate that the integrated system based on thermochemical water splitting can be at least 5% more efficient in exergy terms than the one based on the electrolyzer.

An additional example is illustrated in Fig. 12.11, which shows two integrated multigeneration systems for power, heating, cooling, and desalination. The products are nine in number: electric power, hydrogen, oxygen, drinking water, salt, hot water, space heating, process cooling (e.g., food refrigeration), and air conditioning. The inputs are two: solar energy (which drives the process) and brine. Two implementations of the system are suggested: (a) using the electrolyzer and (b) using the thermochemical water splitting process. The multigeneration exergy efficiency of these systems is given by

$$\psi = \frac{\dot{W} + \dot{Q}_{HW}(1 - T_0/\bar{T}_{HW}) + \dot{Q}_{SH}(1 - T_0/\bar{T}_{SH}) + \dot{Q}_C(1 - T_0/\bar{T}_C) + \dot{Q}_{AC}(1 - T_0/\bar{T}_{AC}) + \dot{E}_S}{I_{sun}(1 - T_0/T_{sun})},$$

(12.16)
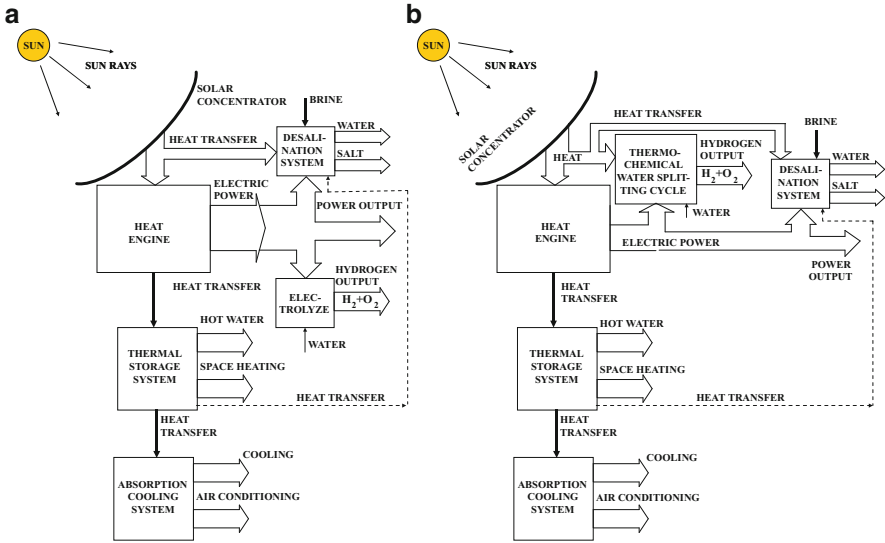
Fig. 12.11 Hybrid solar multigeneration systems with hydrogen production and desalination using high temperature electrolysis (**a**) and thermochemical water splitting process (**b**)

where the meaning of the indexes are the same as above, and "S" stands for "salt." The process (b) uses high-temperature heat to drive water splitting, desalination, and the heat engine; thus, this system generates less electricity than system (a), which uses high-temperature heat only for the heat engine and for desalination. Using Eq. (12.16), the multigeneration exergy efficiency of system (a) is theoretically estimated to be 45%, while that of system (b) is estimated to be 50%.

12.4 Hybridization

The examples above refer to integrated multigeneration systems that are able to generate multiple products from a primary energy source of a single kind. There is also potentially more benefit if the system is engineered to produce outputs from multiple kind sources. Thus, systems can be devised to generate power from wind and solar simultaneously, or generate power and heat from geothermal and solar source, or from biomass combustion and solar source. A typical case entails solar electric generation systems that integrate concentrated solar collector technology with advanced Rankine generators and with natural gas steam generators for backup power. Such systems are called hybrid.

Hybridization of conversion systems involves coupling various technologies together to extract useful energy system from sources that are fundamentally different, with the purpose of obtaining better utilization factors and better effectiveness than that of the integrated systems that use one single kind of primary energy. Obviously, hybrid systems can be devised to generate multiple products.

We demonstrate in this section the benefit of hybridization through an illustrative example that integrates solar and geothermal energy to generate absorption cooling. Absorption cooling systems (ACSs) have become suitable for producing an inexpensive heat energy source over 65°C. Therefore, geothermal and solar energy have a wide range of application potentials for cooling. In the example presented here, the Bigadic geothermal field is selected; this site is located about 38 km south of Balikesir Province, situated in the western part of Turkey. The well head temperature is 98°C, and the geothermal fluid temperature, entering the heat exchangers constructed under each house, changes between 65° and 80°C depending on the operating condition in the system. The ACS utilizes a solution of lithium bromide (LiBr) and water under a vacuum as the working fluid. The absorption cycle is energized by hot water at 85° to 95°C. In the system, the LiBr–water solution temperature is increased to 85° to 95°C by using solar energy.

The following assumptions are made in energy and exergy analyses for the LiBr–water refrigerant system:

- Heat and pressure losses in all the heat exchangers and the pipelines are negligible.
- The reference state temperature and pressure for the system is chosen as 25°C and 101 kPa.
- The temperature of the solution entering the throttle valve is checked by using the EES program to avoid crystallization.
- The solution in the generator and the absorber are assumed to be in equilibrium at their respective temperatures and pressures.
- Water at the condenser and evaporator exit is in a saturated state.
- The strong solution of the refrigerant leaving the absorber and the weak solution of the refrigerant leaving the generator are saturated.

The energy balances for the condenser, evaporator, absorber, generator, and heat exchanger are given (per unit of mass basis) in the following equations (Fig. 12.12):

For the condenser,

$$Q_{con} = m_{water}(h_8 - h_9) = m_{con}(h_{19} - h_{18}). \tag{12.17}$$

For the evaporator,

$$Q_{ev} = m_{water}(h_{11} - h_{10}) = m_{ev}(h_{16} - h_{17}). \tag{12.18}$$

For the absorber,

$$Q_{abs} = m_{water} \cdot h_{11} + m_{WS} \cdot h_7 - m_{SS} \cdot h_1 = m_{abs}(h_{15} - h_{14}). \tag{12.19}$$

For the generator,

$$Q_{gen} = m_{WS} \cdot h_5 + m_{water} \cdot h_8 - m_{SS} \cdot h_4 = m_{gen}(h_{20} - h_{21}). \tag{12.20}$$

Fig. 12.12 Hybrid solar and geothermal-driven absorption cooling system [modified from Coskun et al. (2010)]. *HE* heat exchanger

For the heat exchanger,

$$Q_{\text{geo}} = m_{\text{SS}}(h_4 - h_3). \tag{12.21}$$

Collector efficiency is a major indicator in the conversion process of solar energy to thermal energy. To find the converted energy in the solar collector, collector efficiency should be determined for each possible condition. It is known that many parameters affect the energetic and exergetic efficiencies of thermal collectors. Some of them can be expressed as the intensity of the solar irradiance, outdoor temperature, and input–output feed water temperature. The evacuated vacuum tube type collectors should be utilized effectively to achieve a higher water temperature. Thermal collector efficiency changes with the intensity of the solar irradiance (I), outdoor temperature (T_0), and input–output feed water temperature (T_{in}, T_{out}).The formulation of the energy efficiency characteristic is given in the following equation:

$$\eta_{\text{coll}} = 0.83 - 2.19 \times \frac{(T_{\text{in}} + T_{\text{out}})/2 - T_0}{I}. \tag{12.22}$$

Coskun et al. (2010) introduced the *geothermal–solar energy fraction* (GSEnF), a parameter expressed as the fraction of the geothermal energy to solar energy utilized in the system:

$$GSEnF = \frac{E_{\text{geo}}}{E_{\text{solar}}}, \tag{12.23}$$

where E_{solar} and E_{geo} represent the solar and geothermal energy inputs for cooling. Geothermal energy input throughout the daytime varies between 20% and 8% of total energy input for $2°$ to $18°C$ evaporator temperature variation. The GSEnF varies between 0.08 and 0.24 for investigated system. It decreases with increasing evaporator temperature. In addition, GSEnF also decreases with decreasing absorber temperature. The analysis results show that GSEnF gives the same value (0.10) for a $14°C$ evaporator temperature, although the absorber temperature varies.

Another parameter, the geothermal–solar exergy fraction (GSExF), is expressed as the fraction of the geothermal exergy to solar exergy utilized in the system:

$$GSExF = \frac{Ex_{\text{geo}}}{Ex_{\text{solar}}}, \tag{12.24}$$

where Ex_{solar} and Ex_{geo} represent the solar and geothermal exergy inputs for cooling. The GSExF is investigated for different working conditions, and the results are given in Fig. 12.13. Exergy input from geothermal sources is very low level and it varies between 0.1% and 1% of total exergy input. The percentage solar energy input rate increases with evaporator temperature. As can be seen in the figure, it decreases with increasing evaporator temperature.
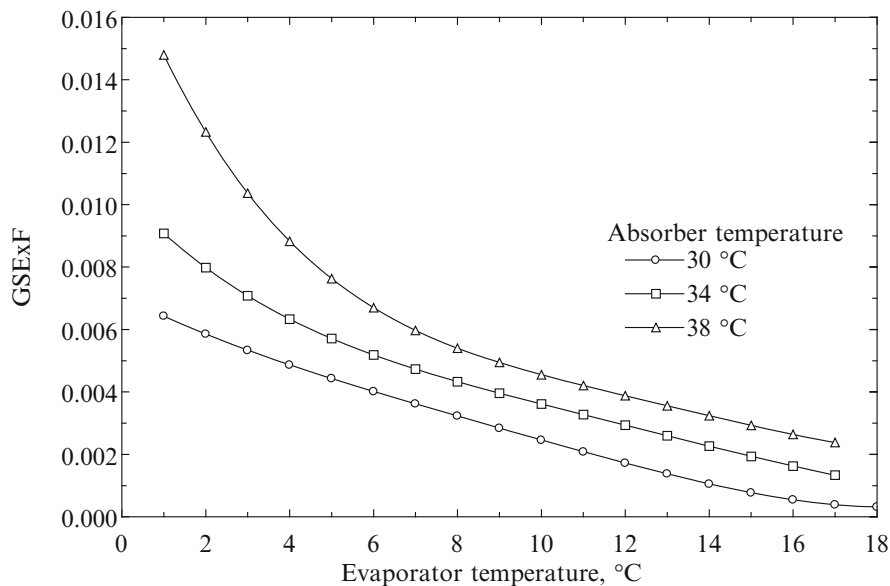
Fig. 12.13 GSExF versus evaporator temperature for different operating conditions [modified from Coskun et al. (2010)]

12.5   Economic Aspects of Multigeneration Systems

Multigeneration systems can be found in many applications, starting with residential settings (where they can be used for generation of power, heating, and cooling, for example) and ending with industrial parks or agricultural farms. Their successful integration within a larger process requires detailed information regarding the energy consuming technologies to be desired and the availability of primary energy resources. It is important that all technical information regarding energy demand be organized in a working model that allows for the effective design of the multigeneration system. Walker (1984) provided a general method for the analysis and design of integrated energy systems; the primary application is in agricultural settings, but the method is more general and can be used to design an integrated multigeneration energy system for any kind of application.

Design engineers must address logistical, environmental, and economic problems with regard to the integration of energy systems in agricultural, industrial, commercial, and residential settings. When analyzing the integration of multigeneration energy system in a given setting, one first has to study the involved technological processes, which for an industrial or agricultural setting can be classified into three categories: material transformation, material transport, and material storage. Residential and commercial settings are different, even though their energy needs consist mainly of electric power, space heating, hot water, air conditioning, and cooling (e.g., for water cooling, ice making, or food preservation). These needs are present also in industrial and agricultural settings;

in the above three category classifications, they can be assimilated to the material transformation category. With any phase of the process there are associated costs. Three main categories of costs are identified in Walker (1984): land, labor, physical energy costs. Depending on the case, there also may be other costs relevant to the analyses. For multigeneration systems, specific costs eventually can be assigned for any kind of output. In the cost assignment process, one must account for all categories of costs involved.

In the multigeneration example suggested in Fig. 12.11, the value of the drinking water is not accounted for in the utilization and exergy efficiency equations; it cannot be! This is because water has no energy value. Moreover, for the same reasons, in the systems that generate hydrogen and oxygen from water, the water itself cannot be considered in energy/exergy efficiency or as an input. However, water, even in abundance, is not free. This reasoning leads to the conclusion that the performance of multigeneration energy systems must be evaluated from the economic point of view, in addition to the performance defined through thermodynamics. The "economic effectiveness" of an integrated multigeneration system can be estimated by the following equation:

$$Ee = \frac{\sum_i C_{o,i}}{C_{PF} + \sum_j C_{m,j}}, \tag{12.25}$$

where $C_{o,i}$ is the monetary cost of the output i, C_{PF} is the monetary cost of the primary fuel, and $\sum_j C_{m,j}$ is the total cost of materials input in the process. The cost of products in the numerator of Eq. (12.25) can include only the benefit part and exclude the part used for amortization of the investment in the multigeneration equipment.

For a simple cogeneration system, the economic effectiveness includes the costs associated with electric and thermal energy and the cost of fuel. If the system is more complicated, advanced economic calculations must be performed to determine the economic effectiveness. The problem becomes more complicated if economic incentives that help financing are available. Cogeneration (CHP) projects are generally recognized by governments and other financing bodies as drivers toward better sustainability and a healthier environment; therefore, at present there is relevant experience in financing those projects.

Through financing, both the capital cost and the price of products (like the kWh of power or thermal energy) can be made more favorable so that the economic effectiveness of the cogeneration system is increased. Hamrin (2005) describes the financing system of cogeneration projects in California. There, the Public Utility Regulatory Policy Act established in 1978 has been prolific in encouraging cogeneration, which increased in the market from virtually nil to a multimillion dollar business in about 10 years. Several types of financing were used both in the United States and in the European Community (See Fee 2005):

- Innovative vendor financing such as financial savings guarantees, package financing, shared savings contracts, and vendor-backed equipment leasing

- Third-party financing
- Energy project or utility financing

The legal framework regarding the encouragement of cogeneration (CHP) plants differs from country to country. Some countries allow the installer of the CHP system to sell back electricity to the grid at a favorable price so that the producer can make a profit; other countries do not encourage this kind of business. Here are some financing examples from various countries, as taken from Fee (2005), that reflect the situation:

- *Canada*: Only Alberta offers the right to sell back to the grid; Ontario and British Columbia implemented policies of "encouraging" sales to the grid. The tariffs for electricity sold to the grid in Alberta are established at the provincial level only. In Ontario, the power utility can affiliate with local energy producers and buy the electricity produced by them.
- *United States*: Energy auto-producers have the right to sell electricity to the grid at a fixed tariff and the grid has an obligation to buy. The rates are set by the state's public utility commission. Some states give local producers the right to sell electricity to third parties while other states do not.
- *Sweden*: Energy auto-producers have the right to sell electricity to the grid at a fixed tariff and the grid has an obligation to buy. The profit is equally shared between the seller and the buyer.
- *Austria*: Auto-producers have the right to sell to the grid only where the power is in surplus to their own use. The tariff is aligned with the State Power Board's wholesale tariff in a range of 80% to 100% of the energy charge of the wholesale tariff.

The usual practice regarding the financing of cogeneration systems is by either purchasing the equipment or by leasing it for a period of 3 to 7 years (Kolanowski 2008). An important factor in financing multigeneration projects is represented by the reduction of greenhouse gas emissions that these systems are capable of with respect to other systems. The expected reduction in CO_2 emissions as a result of using tri-generation and cogeneration plants is 170 Mt/year in 2015, while in 2030 the expected reduction is 950 Mt/year (International Energy Agency 2008).

The cost-effectiveness of any multigeneration system is directly related to the amount of power it can produce for a given amount of other products such as process heat and cold. For tri-generation systems, one can define the electrical to thermal energy ratio (R_{ET}) as an important performance assessment parameter.

Illustrative Example: Hybrid Solar–Natural Gas System

Let us consider a hybrid solar–natural gas system that is intented to provide heating to a residence, such as a house. The residence is connected to the natural gas network. During the daytime, it uses concentrated solar power to generate steam and reform methane to hydrogen. Thus, during the day, the supply of heat is obtained by combusting hydrogen combined with natural gas. The energy harvested from the sun diminishes the consumption of natural gas. During the nighttime,

when no hydrogen is generated, the heating is obtained by the combustion of natural gas only. Natural gas can be converted to hydrogen by adding steam according to the overall reaction $CH_4 + 2H_2O \rightarrow CO_2 + 4H_2$, which needs 48.3 MJ/kmol of hydrogen.

Assume that the solar collector has a 10 m² aperture area; if 5 kWh/m² day is the the average solar radiation, then the incident radiation is 50 kWh/day. Assuming 10% losses through optics and heat transfer, the amount of harvested heat is 45 kWh/day or 162 MJ. Thus, one can produce $162/48.3 = 3.35$ kmol hydrogen per day, which is 6.7 kg. This hydrogen comes from about 0.7 kmol of natural gas or the equivalent of 0.5 GJ, which costs about \$5. The total thermal effect generated by combustion of 6.7 kg of hydrogen is about 950 MJ. Thus, the cost of heating becomes \$5/950 MJ = \$5.3/GJ. If the same heat is generated by combusting natural gas only, the cost is the same as that of natural gas, which is taken as \$10/GJ. Therefore, the savings resulting from using the hybridized solar–natural gas system is 47%.

12.6 Case Studies

12.6.1 Power, Hydrogen, and Oxygen Multigeneration Using Nuclear Energy

This example, which is based on Zamfirescu et al. (2010), examines the multigeneration of power, hydrogen, and oxygen as a way of upgrading the exergy efficiency of nuclear reactors. The tri-generation exergy efficiency can be calculated in this case with the following equation:

$$\psi = \frac{\dot{W} + \dot{m}_{H_2}\left(ex_{H_2}^{ch} + ex_{H_2}^{P}\right) + \dot{m}_{O_2}\left(ex_{H_2}^{ch} + ex_{H_2}^{P}\right)}{\dot{m}_U ex_U^{ch}}, \qquad (12.26)$$

where superscript ch indicates chemical exergy and exponent P indicates thermomechanical exergy due to pressurizing the product gases for storage.

Consuming the electrical energy produced by the nuclear power plant for water electrolysis and hydrogen cogeneration would not augment the overall exergy efficiency; therefore, this is not the appropriate option for multigeneration. In contrast, recent advances in thermochemical water splitting at intermediate temperatures would enhance the exergy efficiency by recovering heat from a nuclear plant to drive a Cu–Cl system for water splitting and hydrogen and oxygen generation (see Naterer 2008 and Naterer et al. 2009; also detailed in other chapters of this book). Thermochemical water splitting cycles are a promising alternative to electrolysis because they require little or no electricity. If the electricity generation efficiency (about 25% for typical power plants, including average grid loses) and
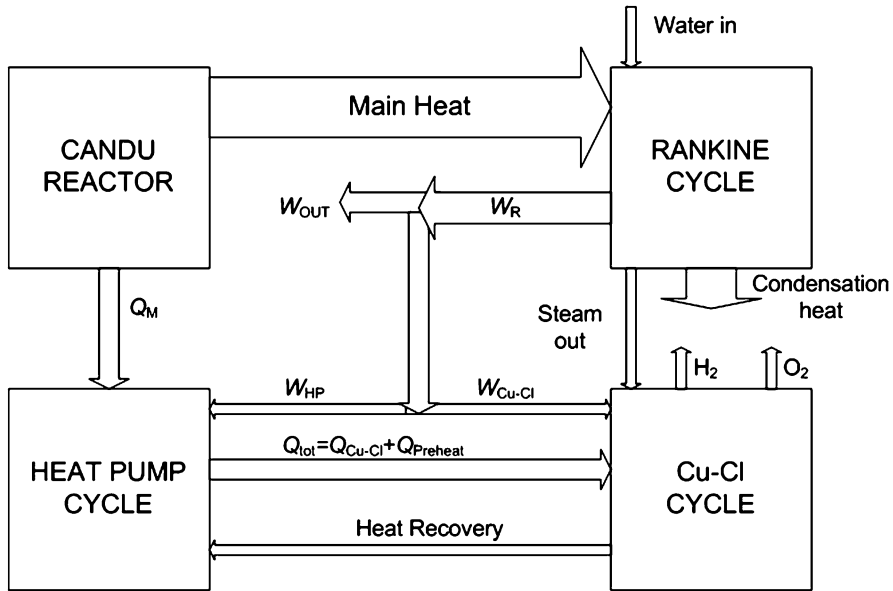
Fig. 12.14 Nuclear reactor multigeneration system for power, H_2 and O_2. *W* work; *Q* heat. Indices: *M* moderator; *R* Rankine; *tot* total; *Cu–Cl* reaction heat [modified from Zamfirescu et al. (2010)]

electrolyzer efficiency (typically about 80% grid-to-hydrogen) are multiplied, the overall efficiency of electrolysis becomes about 20%.

The system configuration presented here utilizes waste heat from a CANDU nuclear reactor, at ~80°C from the moderator vessel, to drive various processes in the Cu–Cl cycle for hydrogen production. Figure 12.14 presents a system that couples a heat pump, Cu–Cl cycle, and a nuclear power plant with the aim to enhance the exergy efficiency of the power plant alone, via multigeneration of hydrogen, oxygen, and power.

The original power plant is a typical nuclear CANDU reactor and represents the reference case. Mainly, a CANDU power plant comprises the nuclear reactor with its moderator circuit, which ejects the moderator heat to the environment and, with the coupled steam generator, produces steam to be expanded in the multi-pressure Rankine power plant. For safety reasons, CANDU power plants are placed in the vicinity of large lakes, which can provide a cooling sink for the condenser. However, the heat from the moderator is at a temperature too high (>60°C) to be ejected into a lake without affecting the ecosystem. With the technology available in the past decade, this temperature is not sufficient to justify the conversion of the moderator heat into work through a heat engine. The practical solution that ensures also the safety of the reactor is to use cooling towers. The proposed method for making use of the heat ejected by the moderator is by coupling the CANDU

Table 12.2 Case study results for the integrated multigeneration for nuclear power, H_2, and O_2

Item	Value (MJ/kmol H_2)	Remarks
Exergy of produced hydrogen	236	At 70°C and 1 bar, as delivered by Cu–Cl plant
Exergy of stored hydrogen	240	Stored in metal hydrides at 14 bar and 20°C
Compression of H_2	7	Electrical power is spent; ideal compression process
Exergy of produced oxygen	2	At 70°C and 1 bar, as delivered by Cu–Cl plant
Exergy of compressed oxygen	122	Stored in cylinders at 200 bar and 20°C
Compression of O_2	107	Electrical power is spent; ideal compression process
Electricity supplied to Cu–Cl plant	140	Spent from the power plant electricity generation
Heat supplied to Cu–Cl plant	179	Comes from the Cu–Cl cycle analysis
Heat extracted from the moderator	188	Comes from heat pump analysis, where $QM = 105\% \ Q_{reaction}$
Generated nuclear heat	3,760	Assumes that all moderator heat is used and this is 5% from generated nuclear heat
Generated power	1,316	Assumed 35% power plant efficiency
Power consumed by heat pump	35.8	Assumed COP = 5
Total consumed power	290	Compressing gases, running the heat pump and Cu–Cl plant
Net power generated	1,026	Total generation minus consumption
Total useful exergy	1,388	See Eq. (12.1)
Carnot factor for nuclear energy	0.52	T_0 is assumed as 26°C and the nuclear reaction temperature $T_N = 350°C$
Consumed exergy	1,950	Based on specific exergy of nuclear fuel
Exergy efficiency with multigeneration	71%	Calculated with Eq. (12.18)

Data from Zamfirescu et al. (2010)
COP coefficient of performance

power plant moderator with the water splitting cycle through the system, as shown here in Fig. 12.14. The three system components are as follows:

1. Rankine cycle (i.e., the power plant that is coupled to the nuclear reactor): low pressure superheated steam is extracted from the Rankine cycle and expanded to 1 bar pressure in the Cu–Cl plant.
2. Heat pump cycle: upgrades the temperature of waste heat from the moderator vessel and consumes electricity, indicated by W_{HP}.
3. Cu–Cl cycle: supplied with electricity by the Rankine generator to drive the electrochemical reaction and compress/store the produced hydrogen and oxygen. The total heat received by the Cu–Cl plant from the heat pump comprises the heat needed to supply the chemical reactions (indicated by $Q_{Cu–Cl}$) and the heat used for reactant preheating.

The predicted results of this case study and the relevant assumptions and comments are presented in Table 12.2. The calculations are scaled for 1 kmol of produced and stored hydrogen. The exergy efficiency of the multigeneration plant

(which recovers and uses the moderator's heat) is improved by 4%, with respect to exergy efficiency of the original power plant (which rejects the moderator heat to the environment), that is, 71% vs. 67%.

The assumptions and calculations for the case study represent the approximate estimates. They represent the first evaluation of the newly proposed multigeneration plant and encourage detailed studies for further confirmation. Based on these results, more improvement in exergy efficiency can be obtained if additional waste heat is recovered to generate electricity.

12.6.2 Integration of SOFC and Rankine Cycles for Tri-Generation

This case study is based on the work of Al-Sulaiman et al. (2010), who proposed and analyzed an integrated tri-generation system comprising a solid oxide fuel cell (SOFC) coupled with a Rankine cycle for producing power, heating, and cooling. The proposed system consists of an SOFC, an organic Rankine cycle (ORC), a heating process, and a single-effect absorption chiller, as shown in Fig. 12.13. The waste heat from the SOFC is used to heat the organic fluid in the ORC. Consecutively, the waste heat from the ORC is used for heating and cooling. The waste heat from the ORC is used to produce steam in the heating process, using a heat exchanger, and to produce cooling, using a single-effect absorption chiller. To have an efficient ORC, the working fluid in the ORC should have a high critical temperature so that usable waste heat can be gained. One of the typical organic fluid types used to operate the ORC is *n*-octane, which has a relatively high critical temperature, 569 K. Hence, it is selected as the working fuel of the ORC.

The assumptions for steady-state modeling of the cycle include the following: efficiency of the ORC turbine and pump of 80% (both), effectiveness of the ORC boiler of 80% and of the solution heat exchanger of the absorption refrigerator of 70%, electric generator efficiency of 95%, dc–ac inverter efficiency of the SOFC of 95%, fuel utilization factor in the SOFC of 85%, and inlet stream temperature of the SOFC of 1,000 K.

Here, the fuel cell is modeled using steady-state gas concentration, Nernst voltage, and the loss voltage, which include ohmic, activation, and polarization losses. Referenced equations are provided in the Al-Sulaiman et al. (2010) study for all voltage components to eventually determine the cell voltage as the difference $V_C = V_N - V_{loss}$. It is assumed that the overall chemical reaction in the fuel cell evolves at equilibrium; based on this assumptions, the molar concentration of the components of the output streams are calculated.

As can be observed in Fig. 12.15, in addition to natural gas, the tri-generation system uses wood as the primary fuel. This should not be considered a variation from the definition of the multigeneration systems that normally use a single kind of primary fuel. Rather, in this case, wood, being a biomass, has the role of
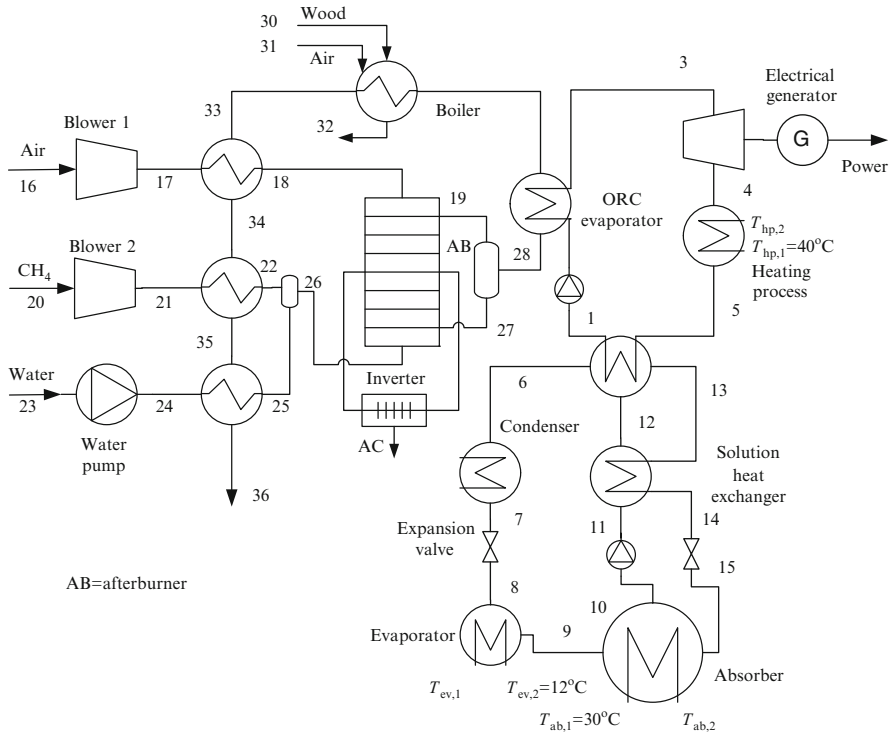
Fig. 12.15 Integrated tri-generation system with SOFC, ORC, and absorption chiller [modified from Al-Sulaiman et al. (2010)]

diminishing the greenhouse gas emissions per unit of useful product. Moreover, burning wood in an externally fired boiler (states 29–33 in Fig. 12.15) is a cheap and well-known technology. Therefore, one considers as the total input exergy in the plant the sum of the exergy consumed from natural gas and from wood: $\dot{E}x_{PF} = \dot{m}_{CH_4} ex_{CH_4}^{ch} + \dot{m}_{wood} ex_{wood}^{ch}$. The tri-generation exergy efficiency becomes

$$\psi = \frac{\dot{W}_{net} + (T_0/T_{ev} - 1)\dot{Q}_{ev} + \left(1 - T_0/\bar{T}_{hp}\right)}{\dot{E}x_{PF}}, \qquad (12.27)$$

where $\dot{W}_{net} = \eta_{inv}\dot{W}_{SOFC} + \eta_{gen}\dot{W}_T - (\dot{W}_{blow,1} + \dot{W}_{blow,2} + \dot{W}_{pmp,w} + \dot{W}_{pmp,ORC})/\eta_{mot}$, T_{ev} is the temperature of the cooling at the evaporator level of the refrigerator, and $\bar{T}_{hp}$ is the average temperature for process heating. Here, one assumes that the plant heats a water stream that enters the heat exchanger at 40°C. The current density, the inlet flow temperature in the SOFC, the pressure inlet of the turbine, and the inlet temperature of the ORC pump are important parameters to be studied.
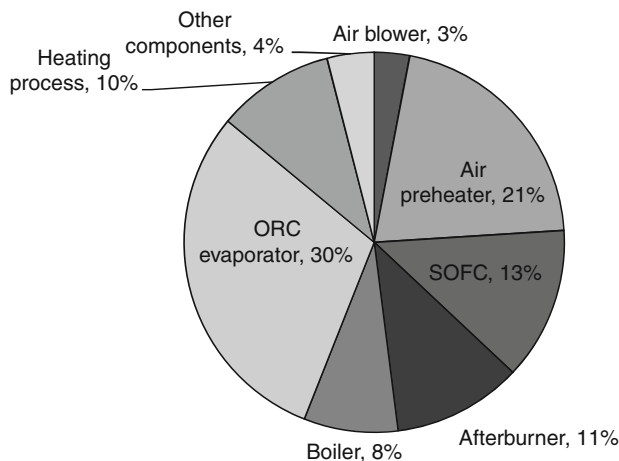
Fig. 12.16 Exergy destruction in percentage for different plant components at 0.75 A/cm^2, 16 bar ORC high pressure, 1,000 K at SOFC inlet, and $T_1 = 345$ K [data from Al-Sulaiman et al. (2010)]
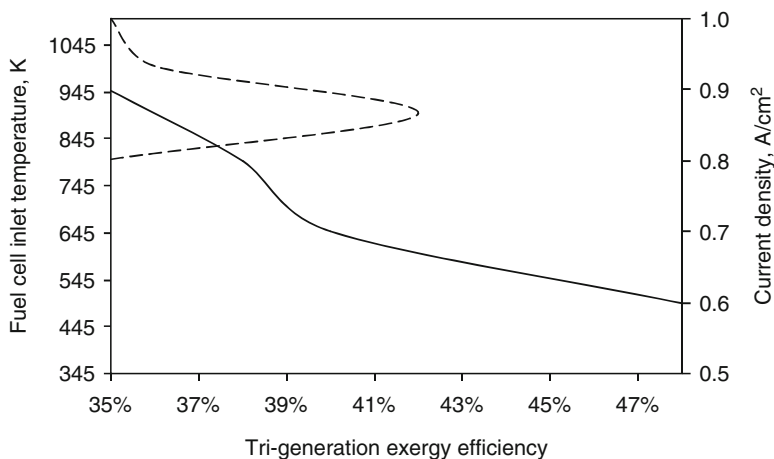
Fig. 12.17 The effect of fuel cell inlet temperature and current density on the overall tri-generation exergy efficiency [data from Al-Sulaiman et al. (2010)]

The calculated exergy efficiency of the tri-generation system varies between 35% and 45% depending on the fuel cell current density (0.6–0.9 A/cm^2) and the inlet flow temperature in the SOFC (800–1,100 K). For an average current density of 0.75 A/cm^2, the exergy destruction rate in percents of the total are given in Fig. 12.16.

The parameters that most affect the overall exergy efficiency are the current density and the fuel cell inlet temperature. The correlation between exergy efficiency and these parameters can be seen from the plot shown in Fig. 12.17.

According to Al-Sulaiman et al. (2010), the gain in the exergy efficiency when tri-generation is used compared with only a power cycle is from 3% to 25%, depending on the operating condition.

12.6.3 Tri-Generation System with Combined Brayton and Absorption Cycles

This case study presents a tri-generation system comprising two Brayton cycles and an LiBr/H$_2$O absorption refrigeration cycle. One of the Brayton cycles works as a refrigerator and is applied for compressor inlet air cooling. The second Brayton cycle is a gas turbine power generator. A heat recovery steam generator (HRSG) for process heat is used in addition to absorption refrigeration for cold production. This system is shown in Fig. 12.18.

The power cycle labeled 1–2–3–4 consists of a compressor, a combustion chamber, and a turbine, and the reverse Brayton refrigeration cycle 1–6–7–8 consists of a cooling coil and an expansion device. A common compressor is used by both the cycles, where the working fluid is divided between the two cycles. A portion of the compressed air $\alpha \dot{m}_1$ at pressure P_6 is extracted, cooled in a heat exchanger to T_7, and then expanded to the atmospheric pressure at T_8. The hot ambient air at T_0 mixes with the cold stream at T_8 before entering the compressor. Owing to the mixing of cold air at T_8 with that at T_0, the temperature at the compressor inlet drops. The expanded gas in the turbine at label 4 is utilized in the HRSG to generate process heat.

The water vapor mixture that enters the evaporator at label 11 is boiled and exits the evaporator in a saturated state at label 12. The saturated steam at label 12 enters the absorber, where it mixes with a solution leaving the generator that is weak in refrigerant and strong in absorbent at label 18, generating heat that has to be dissipated to increase the efficiency of mixing process.

For thermodynamic modeling, mass, energy, and entropy balances are written for each component of the system. In the mixing chamber it is assumed that a 2% pressure drop takes place. The compression process is assumed polytropic. An equation similar to that in the cases above is applied to calculate the tri-generation exergy efficiency. Additionally, the fuel utilization efficiency is calculated as:

$$\eta = \frac{\dot{W}_{\text{net}} + \dot{Q}_{\text{hp}} + \dot{Q}_{\text{C}}}{\dot{m}_{\text{PF}} \text{HHV}_{\text{PF}}}, \tag{12.28}$$

where PF stands for primary fuel, in this case natural gas, and hp stands for process heating. Also the electrical to thermal energy ratio can be calculated as

$$R_{\text{ET}} = \frac{\dot{W}_{\text{net}}}{\dot{Q}_{\text{hp}} + \dot{Q}_{\text{C}}}. \tag{12.29}$$
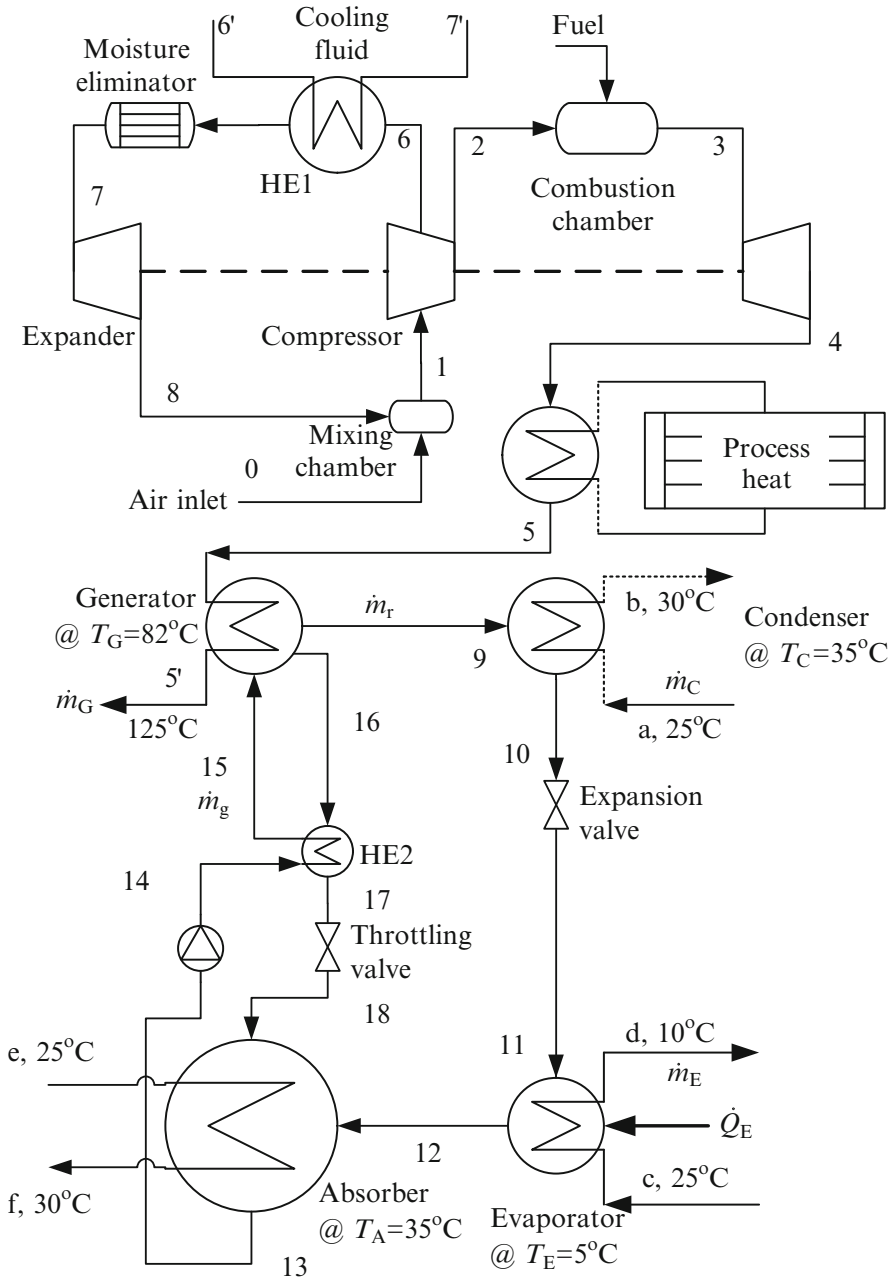
Fig. 12.18 Combined Brayton/absorption cycle tri-generation system with inlet air cooling [modified from Khaliq et al. (2009a)]. *HE* heat exchanger
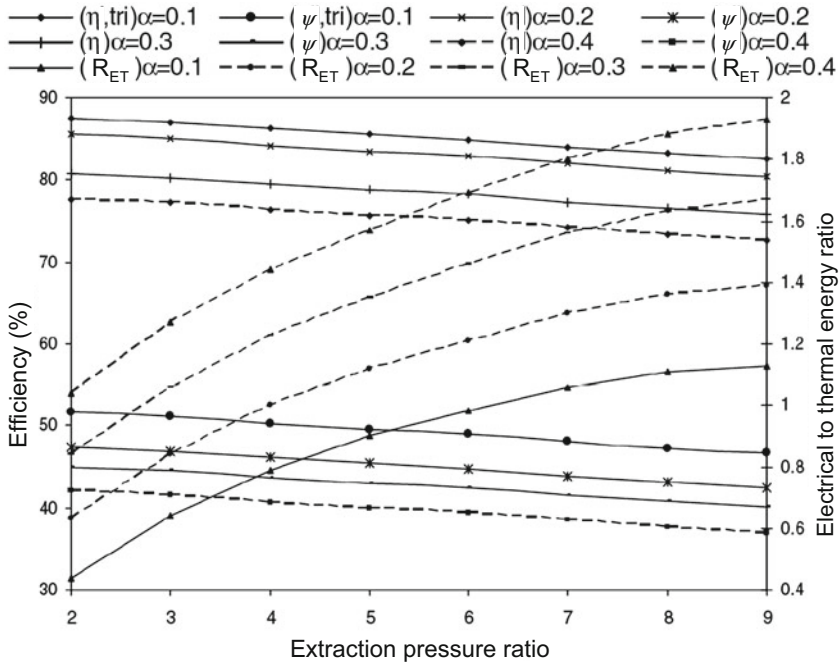
Fig. 12.19 Performance of the tri-generation system expressed as efficiency (utilization and exergy) and electrical-to-thermal ratio as a function of air extraction pressure ratio and α, the air mass flow extraction rate [modified from Khaliq et al. (2009a)]

For the numerical calculation, the inlet air has been assumed at 310 K with 60% relative humidity, the gas turbine pressure ratio has been taken to be 10 with 1,473 K inlet temperature and a fixed specific heat ratio of the combustion gases $\gamma = 1.33$, while for the air compressor process $\gamma = 1.4$. The temperature difference in the heat exchanger is assumed to be 5 K and the pinch point 25 K. With this assumption, the tri-generation efficiency in terms of fuel utilization and exergy, and R_{ET} are reported as a function of the air extraction pressure ratio in the air compressor (defined as P_6/P_1). It can be observed in Fig. 12.19 that the exergy efficiency can reach 50%, while the fuel utilization efficiency approaches 90%.

The performed thermodynamic analysis demonstrates that the utilization and exergy efficiencies increase while the electrical to thermal energy ratio decreases with the extracted mass rate (inlet air cooling). Moreover, the electrical to thermal energy ratio and exergy efficiency are sensitive to process heat pressure, and the process heat pressure should be high for better performance based on the first and second laws of thermodynamics. Regarding the exergy destruction, 21% irreversibility occurs in the combustion chamber, 17% in HRSG, 13.5% in the generator of the absorption refrigeration system, and 12% in the components.

Fig. 12.20 Power and cooling system with combined Rankine and absorption cycles [modified from Khaliq et al. (2009b)]

12.6.4 Integrated Rankine and Absorption Cycles for Power and Refrigeration

This example, based on the work of Khaliq et al. (2009b), is a system for tri-generation that is driven by industrial waste heat available in the temperature range 425–525°C. The system is presented in Fig. 12.20. The waste heat is transferred to the boiler of a steam Rankine cycle, which generates power at its turbine (ST in Fig. 12.20). Further, the hot stream is sent to the generator of an absorption refrigeration machine operating with LiBr/H_2O; the generator is driven with 80°C temperature heat. The cooling effect is obtained at the evaporator of the refrigeration machine.

The thermodynamic analysis indicates that the exergy efficiency is defined in this case with $\psi = \left[\dot{W}_{\text{net}} + \dot{Q}_{\text{C}}(T_0/T_{\text{C}} - 1)\right]/\dot{E}_{\text{PF}}$, where the exergy rate of the primary fuel consumption $\dot{E}_{\text{PF}}$ is calculated as follows:

$$\dot{E}_{\text{PF}} = \dot{m}_{\text{PF}}\{h(T_1) - h(T_0) - T_0[s(T_1) - s(T_0)]\}. \qquad (12.30)$$

The nature of the fluid transferring heat from industry and its associated specific exergy are important. For the range of temperature considered, this fluid is assumed to be a gas. Khaliq et al. (2009b) calculated the efficiency of the cogeneration system for three gases, namely, air, combustion gas with 16.5% oxygen, and combustion gas with 7.5% oxygen. The power-to-cold ratio, defined similarly to the electrical-to–thermal energy ratio—Eq. (12.21)—as the ratio between power output and cooling heat flux output, varies from 2 to 8 for the range of temperature considered. Here, the effect of the considered hot gas stream is minimal. Its effect is also reduced (on the order of 2%) on the value of utilization efficiency, but it is more important on the exergy efficiency, which shows 8% to 10% variation. The highest exergy efficiency is obtained with air and the lowest with the combustion gas with 7.5% oxygen. The exergy efficiency ranges between 35% and 52% depending on the inlet gas temperature. Also the effect of the pinch point in the HRSG has been studied: it is shown that the exergy efficiency varies from 45% to 52% if the pinch point is reduced from 50° to 10°C.

12.6.5 Tri-Generation with Integrated Absorption Refrigeration with Ammonia Turbine

In this case study, an innovative system of generation of power, heating, and cooling that is based on a modified ammonia–water absorption refrigeration cycle that has an integrated power turbine is presented. The cycle is illustrated in Fig. 12.21. It is assumed that the heat source is recovered from an industrial process, and, as in the above example, a combustion gas transfers the heat from the industrial process to the tri-generation unit.

Thermodynamic modeling at steady state has been applied to quantify the system performance. The results shown here are based on the work of Khaliq et al. (2009c). Note that the modified ammonia–water cycle, which incorporates an ammonia turbine, was first proposed by Hasan et al. (2002). The turbine is applied after the ammonia rectification, which is usually done in the ammonia--water absorption cycle. Here, after the rectifier, the resulting high-purity and high-pressure ammonia is superheated. Thereafter, ammonia is expanded in a turbine that operates in two phases. That is, at the turbine outlet one finds an ammonia liquid–vapor at low temperature.
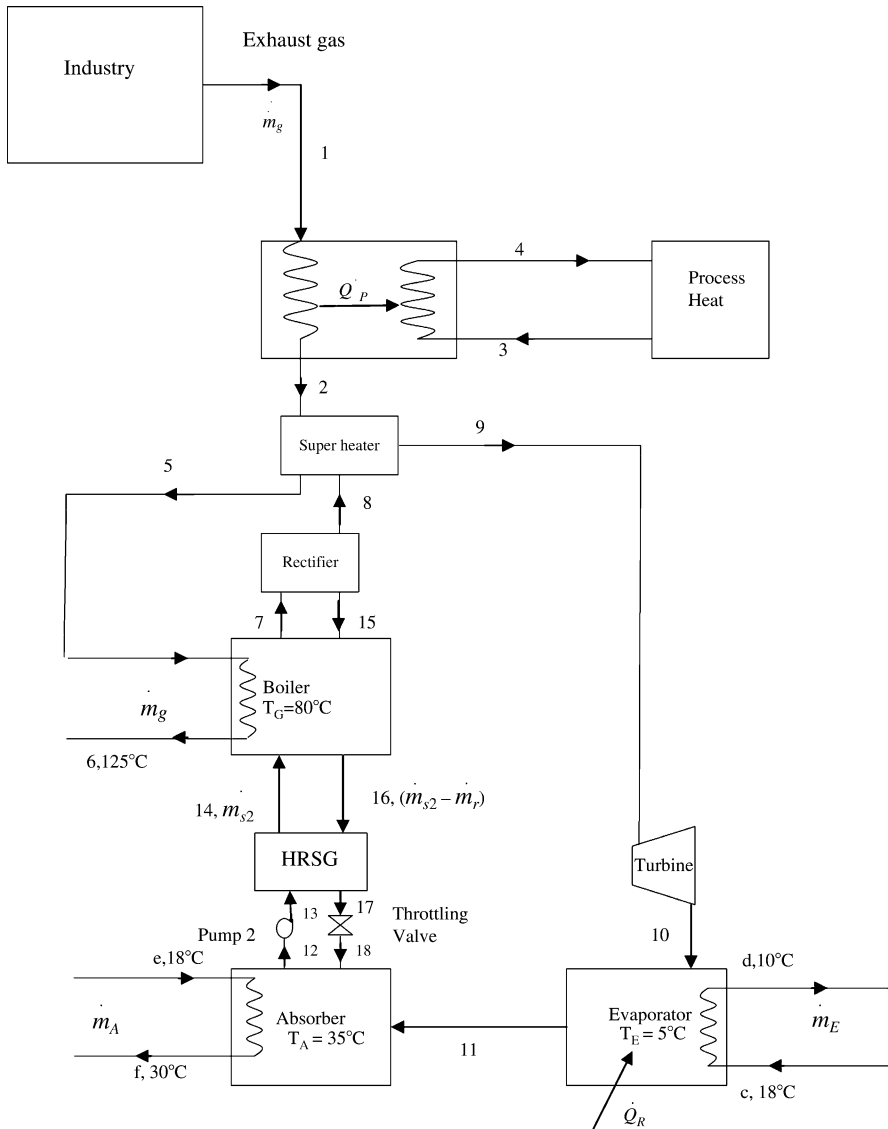
Fig. 12.21 Waste heat recovery driven tri-generation system with ammonia–water [modified from Khaliq et al. (2009c)]

The results show the utilization and exergy efficiency plus the electrical-to–thermal energy ratio as a function of waste heat temperature. The figure ranges between 80% to 85% and 34% to 42% for exergy and utilization efficiency, respectively. The electrical to thermal energy ratio varies from 10 to 20. The considered range of source temperature for the analysis is 375° to 475°C. The process heat is assumed to be used for steam generation (see Fig. 12.21).

The process steam pressure is important because it has an effect on the exergy efficiency of the system. The higher the pressure, the higher the exergy efficiency of the system for a given pinch point. For pressure varying from 10 to 20 bar, the exergy efficiency increases by 10% while the energy efficiency is practically not affected. For the same range of pressures, the electrical-to–thermal energy ratio increases from 8% to 18%.

12.7 Concluding Remarks

This chapter introduced the concept of integrated multigeneration energy systems for practical applications. In a multigeneration energy system, several useful outputs are obtained by using the same input. Such systems offer a wide range of advantages, namely, better efficiency, better cost-effectiveness, better resource use, better environment, and hence better sustainability. Several case studies were presented to highlight the importance of hybrid and integrated multigeneration systems for practical applications.

Nomenclature

C	Specific cost, any currency
Ee	Economic effectiveness
ex	Specific exergy, kJ/kg
Ex	Exergy, kJ
G	Gibbs free energy, kJ/mol
GSEnF	Geothermal-solar energy fraction
h	Specific enthalpy, kJ/kg
HHV	Higher heating value, MJ/kg
H	Enthalpy, kJ
I	Solar irradiance, W
K	Equilibrium constant, Eq. (12.16)
LHV	Lower heating value, MJ/kg
m	Mass, kg
$\dot{m}$	Mass flow rate, kg/s
P	Pressure, bar
Q	Heat, kJ
R	Universal gas constant, J/kmol.K
R_{ET}	Thermal energy ratio
s	Specific entropy, kJ/kg K
S	Entropy, kJ/kgK
T	Temperature, K
V	Voltage, V
W	Work, kJ

Greek Letters

γ Specific heat ratio
Δ Difference
η Utilization efficiency
ψ Exergy efficiency

Subscripts

0   Reference state
abs   absorber
AC   Air conditioning
blow   Blower
C   Cooling or condenser
con   Condenser
d   destroyed
e   Electric
ev   Evaporator
FC   Fuel cell
gen   Generator
geo   Geothermal
H   Heating
hp   Heating process
HW   Hot water
i index
inv   Inverter
j Index
m   Material
mot   Motor
N   Nernst
o   Output
OP   Other product
PF   Primary fuel
pmp   Pump
S   Salt or stack
SF   Synthetic fuel
SH   Space heating
SS   Strong solution
T   Turbine
WF   Working fluid
WS   Weak solution
U   Uranium

Superscripts

ch   Chemical
P   Thermomechanical
(˙)   Rate (per unit of time)
(‾)   Average value

References

Al-Sulaiman F.A., Dincer I., Hamdullahpur F. 2010. Exergy analysis of an integrated solid oxide fuel cell and organic Rankine cycle for cooling, heating and power production. *Journal of Power Sources* 195:2346–2354.

Coskun C., Oktay Z., Dincer I. 2010. Investigation of a Hybrid Solar and Geothermal Driven Absorption Cooling System for District Energy Systems. Second International Conference on Nuclear and Renewable Energy Resources, Ankara, 4–7 July.

Dincer I., Rosen M.A. 2007. Exergy: Energy, Environment and Sustainable Development. Elsevier, Oxford, UK.

Dincer I., Rosen M.A., Zamfirescu C. 2010. Exergetic performance analysis of a gas turbine cycle integrated with solid oxide fuel cells. *Journal of Energy Resources Technology* 131/032011:1–11.

Fee D.A. 2005. Third party financing. In: Combined Production of Heat and Power (Cogeneration), Sirchis J., ed. Elsevier Science Publishing Co., Essex, UK.

Granovskii M., Dincer I., Rosen M.A. 2007. Performance comparison of two combined SOFC–gas turbine systems. *Journal of Power Sources* 165:307–314.

Granovskii M., Dincer I., Rosen M.A. 2008. Exergy analysis of a gas turbine cycle with steam generation for methane conversion within solid oxide fuel cells. *Journal of Fuel Cell Science and Technology* 5/031105:1–9.

Hamrin J. 2005. The history and status of financing cogeneration projects in California with prospects for the future. In: Combined Production of Heat and Power (Cogeneration), Sirchis J., ed., Elsevier Science Publishing Co., Essex, UK.

Hasan A.A., Goswami D.Y., Vijayaraghavan S. 2002. First and second law analysis of a new power and refrigeration thermodynamic cycle using a solar heat source. *Solar Energy* 73:385–393.

International Energy Agency. 2008. Combined Heat and Power: Evaluating the Benefits of Greater Global Investment.

Kanoglu M., Dincer I. 2009. Performance assessment of cogeneration plants. *Energy Conversion and Management* 50:76–81.

Khaliq A., Choudhary K., Dincer I. 2009a. Exergy analysis of a gas turbine trigeneration system using the Brayton refrigeration cycle for inlet air cooling. Proceedings of IMechE Part A. *Journal of Power and Energy* 224:449–461.

Khaliq A., Kumar R., Dincer I. 2009b. Exergy analysis of an industrial waste heat recovery based cogeneration cycle for combined production of power and refrigeration. *Journal of Energy Resources Technology* 131/022402:1–9.

Khaliq A., Kumar R., Dincer I. 2009c. Performance analysis of an industrial waste heat-based. *International Journal of Energy Research* 33:737–744.

Kolanowski B.F. 2008. Small-Scale Cogeneration Handbook: CRC Press, Lilburn CA.

Naterer G.F. 2008. Second law viability of upgrading industrial waste heat for thermochemical hydrogen production. *International Journal of Hydrogen Energy* 33:6037–6045.

Naterer G.F., Suppiah S., Lewis M., Gabriel K., Dincer I., Rosen M.A., Fowler M., Rizvi G., Easton E.B., Ikeda B.M., Kaye M.H., Lu L., Pioro I., Spekkens P., Tremaine P., Mostaghimi J., Avsec J., Jiang J. 2009. Recent Canadian advances in nuclear-based hydrogen production and the thermochemical Cu–Cl cycle. *International Journal of Hydrogen Energy* 34:2901–2917.
Walker L.P. 1984. A method for formulating and evaluating integrated energy systems in agriculture. *Energy in Agriculture* 3:1–27.
Zamfirescu C., Naterer G.F., Dincer I. 2010. Upgrading of waste heat for combined power and hydrogen production with nuclear reactors. *Journal of Engineering for Gas Turbines and Power* 132/102911:1–9.

Study Questions/Problems

12.1 Define the concept of system integration and its benefits. Give practical examples.

12.2 Consider the system from Fig. 12.1. With reasonable assumptions similar to those presented in the chapter, calculate the system efficiency and all state point parameters.

12.3 Explain the concept of multigeneration and its benefits.

12.4 Calculate the system from Fig. 12.7 if the maximum temperature of the working fluid is $400^{\circ}C$ and the minimum is $20^{\circ}C$.

12.5 Calculate the efficiency of the system from Fig. 12.8a that operates with biogas. Make reasonable assumptions.

12.6 Explain the concept of hybridization and its benefits.

12.7 Repeat the calculation for the hybrid system from Fig. 12.12 assuming 5% more solar energy input.

12.8 Devise a hybrid system for biomass and concentrated solar power generation.

12.9 Consider the system from Fig. 12.14; make reasonable assumptions for the efficiency of each component and determine the energy and exergy of the overall system.

12.10 Calculate the cycle from Fig. 12.18 under reasonable assumptions.